GNSS Indoors
Fighting the Fading
Part 2

PROF-DR. GÜNTER HEIN, ANDREAS TEUBER, UNIVERSITY FAF MUNICH
HANS-JÖRG THIERFELDER, ANNE WOLFE, DRESDEN UNIVERSITY OF TECHNOLOGY

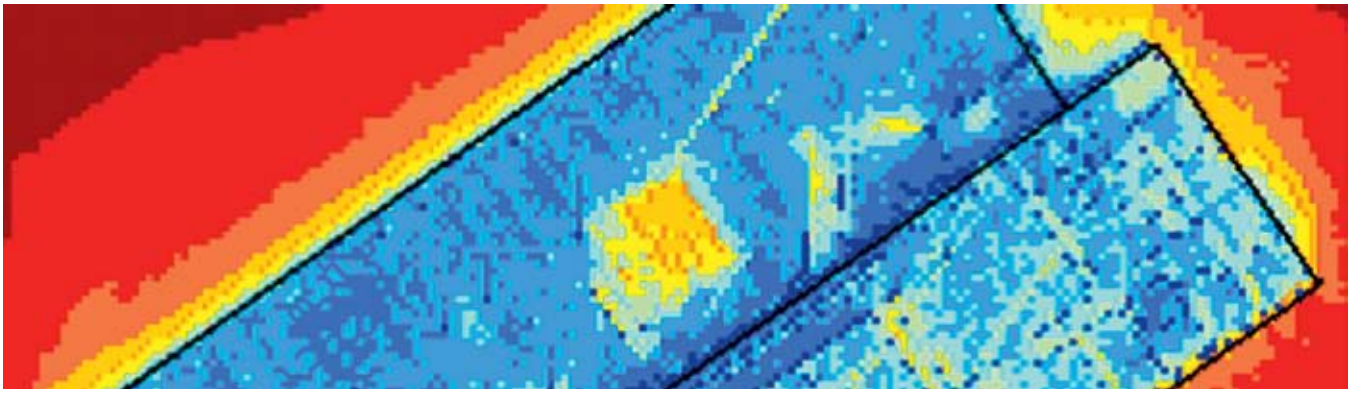

CNES

Finding ways to track GNSS signals inside buildings has taken on some of the qualities of a search for the Holy Grail. Aside from the very low power of the spread spectrum GNSS signals themselves, researchers and product designers face the challenge of sorting out the effects on the signals as they propagate through different architectures and building materials. In this second part of a series, the authors identify and measure some of the key variables affecting signals indoors and outline a transmission model for their behavior.

In Part 1 of the GNSS Indoors column, we described our attempt to establish an indoor channel model that can be applied to GNSS signals. One of the major outcomes of the investigation of channel sounder data was the discovery of a significant dependency on the direction of the signal source. Hence, the azimuth and the elevation of the satellite became key parameters for the indoor channel model.

The granularity of our indoor channel model introduced in Part 1 intentionally did not address the question of the diversified materials used in a building because one statistical model should be able to fit as many conditions as possible. Nevertheless, investigating different building materials with respect to their permeability of GNSS signals poses exciting prospects and will serve as a focus of this second part of the column.

The signal that results from an encounter with the surface of a building material can be divided into a part that is reflected at the boundary and a part that is transmitted through the material. Because the latter signal portion is more interesting in the context of indoor GNSS, we call the model to be developed the *transmission model*. In this second part, some results of the theoretical considerations will be presented as well as some practical test measurements.

Defining a Transmission Model

Modern cities present a large variety of architectural styles, building types, and — as a consequence of these first two factors — of many different materials. Fortunately, due to the activities needed to establish engineering standards, extended databases already exist that contain information on the physical properties of building materials.

Many in the GNSS user community would find it interesting to obtain a consistent description of reflection (including scattering), diffraction, and

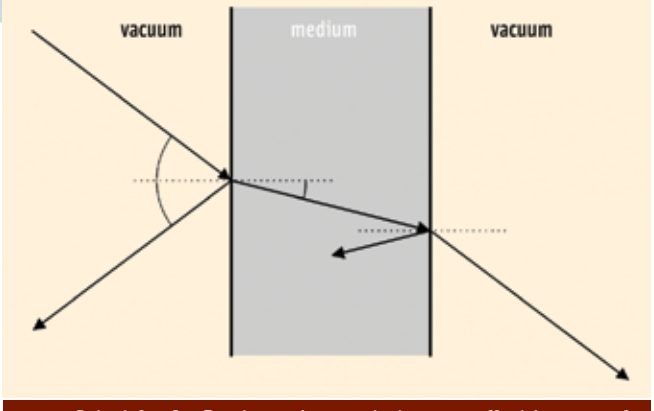

FIGURE 1 Principle of reflection and transmission at a wall with two parallel interfaces

transmission (including refraction) for those materials by accessing the necessary physical parameters.

The standard case of a transmission is depicted in **Figure 1**. The transmission model we will present in the following discussion builds on a geometry-based model that uses the Fresnel equations for reflection and transmission at an interface between two media.

In our investigation we primarily consider straight, plane walls with parallel interfaces and homogenous, nonmetallic materials as well as the attenuation of signals propagating through these walls. Beyond this, we can apply the transmission model to multilayered structures, too. Moreover, the model allows statements about the parallel offset in the path of the signal rays. The model also describes the signal delay caused by refraction at the interfaces and the changed propagation speed inside the material.

Further features of a transmission model include the scattering caused by the roughness of the surface and the influence of intermittent inner structures found in some building materials, for example, the lattice structure of metal reinforcing bars in concrete. The model also takes into account the effect of recurring surfaces on the signal propagation and attenuation.

Media Characteristics

The model assumes that building materials are made up of homogeneous and isotropic media. The latter implies that the properties of the materials are position independent.

These media can be completely characterized by their permeability μ and their complex permittivity $\underline{\varepsilon}$. Note that permeability always refers to the properties of magnetic fields interacting with the material, whereas permittivity deals with the properties of electrical fields associated with the material.

$$\mu = \mu_0 \cdot \mu_r \tag{1}$$

$$\underline{\varepsilon} = \varepsilon_0 \cdot \underline{\varepsilon}_r = \varepsilon_0 \cdot (\varepsilon' + j\varepsilon'') \tag{2}$$

μ_0 and ε_0 denote the vacuum permeability and permittivity, respectively, and μ_r and ε_r the relative permeability and permittivity. The real part ε' of the relative permittivity represents the energy-storing nature of a material whereas the imaginary part ε'' stands for the material's lossy property. For a lossy material we can distinguish between dielectric and ohmic loss.

On Electromagnetic Waves

In the following discussion, GNSS signals are regarded as electromagnetic waves of constant frequency f. At a great distance from their origin, they can be assumed to be plane electromagnetic waves, that is, the wave fronts are infinite parallel planes of constant amplitude orthogonal to the direction of travel.

The electric and the magnetic fields are perpendicular to each other and to the direction of propagation (transverse waves). Additionally, they are in phase in the far field.

Plane electromagnetic waves are solutions of the wave equation:

$$\Delta \underline{\vec{E}} - \mu \underline{\varepsilon} \cdot \frac{\partial^2 \underline{\vec{E}}}{\partial t^2} = \vec{0} \tag{3}$$

The electric and the magnetic field vectors at a given position $\vec{r}$ and a specific time can be denoted as

$$\underline{\vec{E}}(\vec{r}, t) = \underline{\vec{E}}_0 \cdot \exp\left(j \cdot \left(\underline{\vec{k}}\,\vec{r} - \omega\, t\right)\right) \tag{4}$$

$$\underline{\vec{H}}(\vec{r}, t) = \underline{\vec{H}}_0 \cdot \exp\left(j \cdot \left(\underline{\vec{k}}\,\vec{r} - \omega\, t\right)\right) \tag{5}$$

The initial amplitude is given by $\underline{\vec{E}}_0$, $\underline{\vec{H}}_0$ respectively. The angular frequency is ω.

$$\omega = 2\pi \cdot f \tag{6}$$

The wave vector $\underline{\vec{k}}$ specifies the direction of propagation (with unit vector $\vec{n}$) and the wave number $\underline{k}$ representing the material properties.

$$\underline{\vec{k}} = \underline{k} \cdot \vec{n} \tag{7}$$

We obtain the following relation for the wave number by applying the wave equation (3) to the equation of the plane electromagnetic waves (4).

$$\underline{k}^2 = \omega^2 \mu \underline{\varepsilon} = \omega^2 \mu \varepsilon_0 (\varepsilon' + j\varepsilon'') \tag{8}$$

$$\underline{k} = \omega \sqrt{\mu \varepsilon_0} \left(\sqrt{\tfrac{1}{2}\sqrt{\varepsilon'^2 + \varepsilon''^2} + \tfrac{1}{2}\varepsilon'} + j \cdot \sqrt{\tfrac{1}{2}\sqrt{\varepsilon'^2 + \varepsilon''^2} - \tfrac{1}{2}\varepsilon'} \right) \tag{9}$$

If no time dependencies are regarded, equation (4) will reduce to the following expression:

$$\underline{\vec{E}}(\vec{r}) = \underline{\vec{E}}_0 \cdot \exp\left(j \cdot \left(\underline{\vec{k}}\,\vec{r}\right)\right) \tag{10}$$

The propagation speed depends on the material. In vacuum, it is the speed of light

$$c = \frac{1}{\sqrt{\mu_0 \varepsilon_0}} \tag{11}$$

which reduces for propagation in materials to

$$v = \frac{\omega}{\mathrm{Re}\{\underline{k}\}} \tag{12}$$

Because the frequency remains constant, the altered propagation speed is proportional to the change of the wavelength λ:

$$v = \lambda \cdot f \tag{13}$$

Plane electromagnetic waves may be polarized. The polarization describes the direction (or the behavior) of the electric field vector in the plane perpendicular to the direction of travel. We distinguish between linear, circular and elliptical polarization.

We can assume GNSS signals to be right-hand circularly polarized. When electromagnetic waves interact with matter, their direction of propagation and their polarization state may be altered.

Reflection, Refraction and Transmission

At a plane interface between two media, a wave is partly reflected and partly transmitted and refracted. The reflected wave returns into the first medium from which it originated and the transmitted wave travels through the second medium. The reflected and the transmitted wave lie in the plane of incidence described by the wave vector of the incident wave and the normal vector of the interface.

If we know the parameters of the incident wave, the position of the interface between the two media (and therefore the position of the plane of incidence), and the material parameters on both sides of the interface, we can calculate the direction of propagation and the

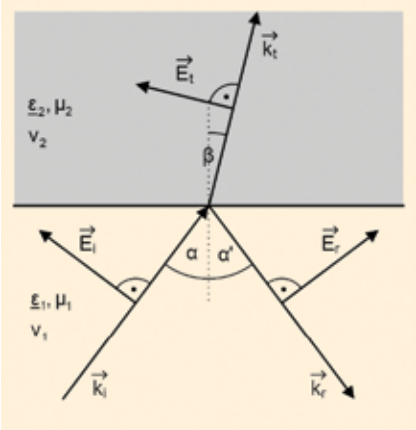

FIGURE 2 Reflection and refraction at an interface between two media

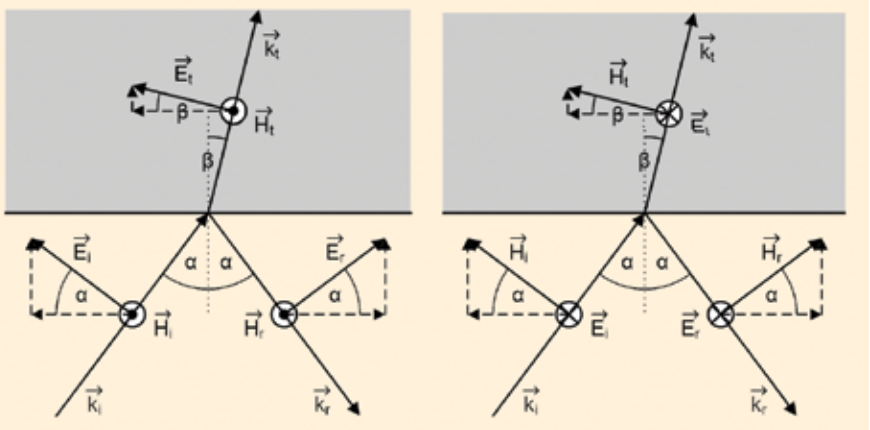

FIGURE 3 Reflection and refraction at an interface between two media for horizontal polarization (left) and vertical polarization (right)

amplitude vector of the reflected and the transmitted wave (Figure 2).

The new propagation direction of the reflected wave can be obtained by the law of reflection. The angle of incidence α and the angle of reflection α' must be the same.

$$\alpha = \alpha' \qquad (14)$$

Both angles are defined between the respective wave vector and the normal vector of the interface in the plane of incidence. The propagation direction of the transmitted wave is defined by the angle of refraction β. β describes the angle between the wave vector and the normal vector of the interface in the plane of incidence and can be calculated by the law of refraction (Snell's law):

$$\frac{\sin(\alpha)}{\sin(\beta)} = \frac{v_1}{v_2} = \frac{\mathrm{Re}\{\underline{k}_2\}}{\mathrm{Re}\{\underline{k}_1\}} \qquad (15)$$

In describing the properties of building materials, the wave impedance $\underline{Z}$ is a useful parameter for ascertaining the amplitudes of the reflected and the transmitted waves:

$$\underline{Z} = \frac{\underline{E}}{\underline{H}} = \frac{\omega \cdot \mu}{\underline{k}} = \frac{\sqrt{\mu}}{\sqrt{\underline{\varepsilon}}} \qquad (16)$$

Two further important parameters are the reflection and the transmission coefficients. The reflection coefficient ρ is defined by the ratio of the amplitudes of the reflected and the incident waves, whereas the transmission coefficient τ is defined by the ratio of the amplitudes of the transmitted and the incident wave. Their values depend on the polarization state of the incident wave.

As mentioned earlier, GNSS signals are right-hand circularly polarized. This means that after a distance of one wavelength the electric and the magnetic field will have executed one full rotation around the propagation direction of the wave front. Two polarization states in particular — the horizontal and the vertical — deserve to be considered exclusively.

Effect of Various Polarization States

If the electric field vector lies in the plane of incidence, we will use the terms horizontal or parallel polarization or *p-like* (see the left side of Figure 3). If the electric field vector is perpendicular to the plane of incidence, we use the terms vertical or perpendicular polarization, or *s-like* (right side of Figure 3). These two cases are sufficient for all possible polarization states of the incident wave as every incident wave may be described as the superposition of two orthogonal basic waves.

Figure 4 depicts the effect of the polarization state on signal waves. Here, the amplitudes of the reflected and transmitted waves relatively to the amplitude of the incident wave are shown for a range of incident angles from 0 to 90 degrees. As the first interface a wall consisting of a lossless material with $\underline{\varepsilon}_r = 3$ is assumed.

Differences between the two elementary polarization states are obvious. For vertical polarization (left graph of figure), the continuity of the tangential electric field components can be identified as well as the Brewster's angle (no reflection at all) for horizontally polarized waves.

In particular, Figure 4 shows that the polarization state is of high importance for the reflected portion of the wave, whereas regarding the transmitted portion the influence of the polarization state is smaller.

Attenuation In a Medium

Waves propagating inside a lossy medium are attenuated. This fact is modeled by the imaginary part of the wave vector:

$$\underline{k} = k_{real} + j \cdot k_{imag} \qquad (17)$$

Applying Equation (4) we obtain an exponential decay of the electric field amplitude over the distance the wave travelled inside the medium.

$$E(r,t) = \underline{E}_0 \cdot \exp\left(j \cdot \left(\underline{k}_{real} \cdot \underline{r} - \omega \cdot t\right)\right) \cdot \exp\left(-\underline{k}_{imag} \cdot \underline{r}\right) \qquad (18)$$

For media with good conductivity, the attenuation is very high. By approximation, we can assume that no wave propagation occurs inside such a medium.

In this article, we shall limit our investigation to the simple considerations introduced to this point. Of course, further considerations — e.g., for multi-layered structures, rough, inter-

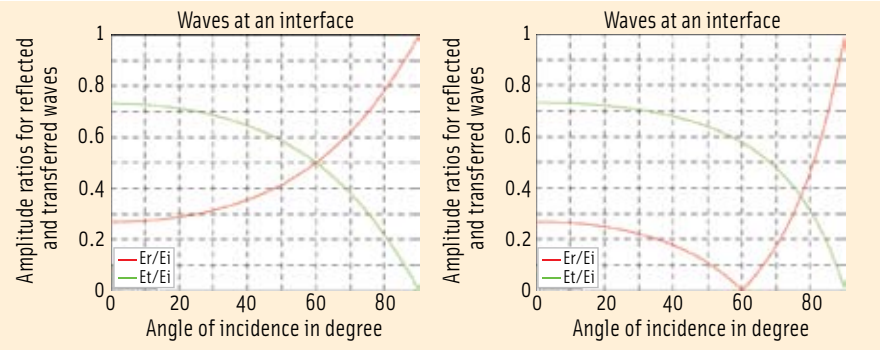

FIGURE 4 Relative amplitudes (absolute values) of reflected wave (red) and transmitted wave (green) at an interface between vacuum and a material with $\varepsilon_r = 3$: vertical polarization (left), horizontal polarization (right)

mittent, or grated surfaces — have been made, leading to a transmission model that could almost serve as an all-purpose model.

Some Simulations

We ran a simulation to determine the effects of different materials on signal reflection, transmission, and attenuation. The selected materials, their thicknesses, and their assumed permittivity parameters are listed in Table 1.

For the simulations, we assumed that the propagated wave enters the building perpendicular to the plane of the boundary layer (incident angle 0°). We conducted a first run on the listed materials for the L1 frequency at 1575.42 MHz with the resulting reflection and transmission coefficients given in Table 2.

From Table 2 we can see that, at an incident angle of 0 degree, in most materials the transmitted portion of the wave is dominant compared to the reflected one, especially for wooden materials such as plywood or lumber. Tinted glass, in contrast, has a very high reflection coefficient.

Comparing the eight selected materials and considering the combined effect of transmission and attenuation, the signal is the weakest after penetrating tinted glass (attenuation of more than 24 dB). When considering the pure attenuation inside the material, the reinforced concrete attenuates the signal even more.

For most of the lighter materials (wood, glass), the reflection is obviously the dominant part that causes loss of signal power — in the case of dry wall, comprising 99 percent —whereas for the more massive materials (brick, concrete) the attenuation taking place inside the medium is dominant.

Does Carrier Frequency Make a Difference?

With the advent of Galileo and modernized GPS the number of carrier frequencies will increase, and a new portion of the L-band — the L5/E5 at a center frequency of 1176 MHz — will be allocated. The frequency separation between L1 and L5/E5 is almost exactly 400 MHz.

While the differences in attenuation that are affecting the two signals on their outdoor propagation paths can be considered as marginal, it is interesting to see whether the properties of indoor transmission will cause a higher impact on the two signals. Table 3 presents the results of simulations comparing the L1 and L5/E5 signals' interaction with various building materials (with the assumption that permittivity parameters remain constant for both frequencies).

The reflection and transmission coefficients are independent of carrier frequency. Thus, the differences seen in Table 3 between L1 and L5/E5 stem from different attenuation properties when traveling through the media: the lower the frequency, the smaller the attenuation. Therefore, materials that already manifest greater effects on signals due to their attenuation coefficients show a significant additional attenuation on the L1 signal compared to the lower frequency L5/E5 (tinted glass, reinforced concrete).

Autonomous Measurements

As mentioned earlier, existing databases provide information on transmission properties of materials that make up a large portion of buildings. These tables typically contain values for the real and imaginary parts of the materials' relative permittivity, ε' and ε'', respectively.

Standardized construction materials — e.g., bricks, lumber panel, plasterboard, elements of reinforced concrete,

Material	Thickness [cm]	e'	e''
Dry wall	1	6	0.1
Plywood	1	1.85	0.35
Glass	0.4	6	0.5
Tinted glass	0.4	1	800
Lumber	10	2.7	0.27
Brick	24	4.2	0.4
Concrete	40	5.5	0.6
Reinforced concrete	40	5	1.27

TABLE 1. Selected building materials, their thicknesses, and their permittivity parameters

L1 signal at 1575.42 MHz	Reflection coefficient ρ	Transmission coefficient τ	Transmission and attenuation coefficient		Pure attenuation inside medium
	[1]	[1]	[1]	[dB]	[dB]
Dry wall	0.4202	0.5788	0.5759	2.40	0.02
Plywood	0.1572	0.8428	0.8079	0.93	0.18
Glass	0.4211	0.5789	0.5712	2.43	0.06
Tinted glass	0.9500	0.0500	0.0036	24.44	11.43
Lumber	0.2446	0.7554	0.5761	2.40	1.18
Brick	0.3453	0.6547	0.3025	5.19	3.35
Concrete	0.4036	0.5964	0.1104	9.57	7.33
Reinforced concrete	0.3899	0.6101	0.0214	16.70	14.55

TABLE 2. Reflection, transmission, and attenuation factors for L1 carrier frequency

or even glass — have a well-defined density and are offered in a limited range of thicknesses. For these various thicknesses an additional value of attenuation can easily be expressed.

However, the compilation of these attenuation values often appears as a mosaic that draws on numerous sources and perhaps even different signal frequencies. Therefore, we would like to present our own measurements dedicated to the L-band and the three Galileo carrier frequencies. To carry out these measurements, we employed three different setups to capture the data.

Case 1: Anechoic Chamber

The first setup was for attenuation measurements recorded in a free-field room or anechoic chamber (Figure 5). A sample of each type of building material under investigation was placed in a measurement window one meter square, which was assembled in the door of the free-field room.

The interior of the chamber — approximately 6 × 6 × 3 meters in size — was completely covered with conical HF absorbers. In order to eliminate influences caused by the near field of the antennas, both the transmitting and receiving antennas were placed at a distance of approximately three meters away from the material sample in the measurement window.

The antennas were relatively wide-banded (3 dB bandwidth from 100 MHz to 2000 MHz), circularly polarized helical L-band antennas. They were specially developed for this purpose and conformed with the conditions for the reception of circularly polarized signals. (The key design criterion was the high bandwidth and not the antenna gain.)

The main item of the measurement instrumentation was a network analyser for the frequency range 10 MHz to 67 GHz. We used a wobble transmitter on the transmitting side and a receiving converter (relocated from the network analyser) on the receiving side to avoid high cable attenuations and radiations of disturbing signals.

All measurements were carried out in the complete L-band, that is, in the frequency range of 1000 MHz to 2000 MHz. With the measurement window open, we calibrated and normalized the complete measurement configuration on a value of 0 dB for the common L-band. The drawback of this setup was the limited size of the measurement window that in turn limits the size of the test material samples. Table 4 shows some of the results from these attenuation tests.

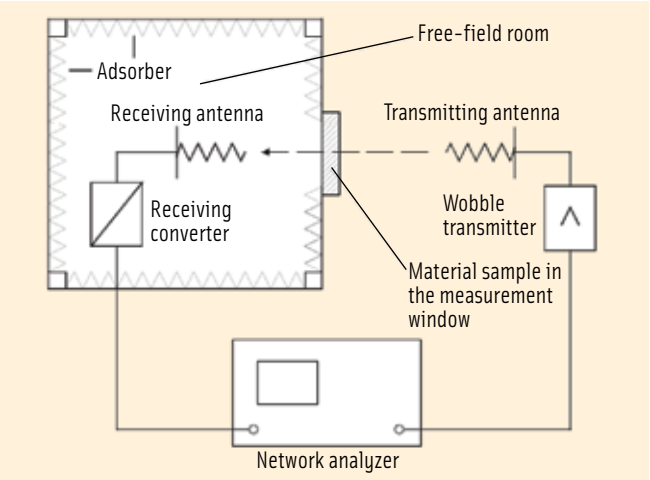

FIGURE 5 Measurement setup in the free-field room

Case 2: In-Building Tests

We next tested attenuation at a selected set of typical locations inside buildings (Figure 6). This required the use of a suite of portable, battery-powered measurement equipment: an L-band generator for the middle frequencies of the three Galileo frequency ranges 1190 MHz, 1280 MHz, and 1575 MHz; a portable spectral analyzer, and the wide-band circularly polarized helical antennas already used for the measurements in the free-field room.

The L-band generator was made up of three independent synthesizers based on programmable integrated circuits and a 10 MHz reference crystal clock circuit. The output signals of the synthesizers were led via programmable attenuators and a combiner circuit to the output of the generator. The maximum power for each of the three signals in the frequency range 1100 MHz - 1700 MHz was 10 dBm. The implemented rechargeable battery pack allowed continuous operation for at least 10 hours.

Comparison L1 / L5/E5	Transmission & attenuation coefficient L1	Transmission & attenuation coefficient L5/E5	Pure attenuation inside medium L1	Pure attenuation inside medium L5/E5	Additional attenuation at L1
	[dB]	[dB]	[dB]	[dB]	[dB]
Dry wall	2.40	2.39	0.02	0.01	0.01
Plywood	0.93	0.88	0.18	0.13	0.05
Glass	2.43	2.42	0.06	0.05	0.01
Tinted glass	24.44	21.55	11.43	8.54	2.89
Lumber	2.40	2.10	1.18	0.88	0.30
Brick	5.19	4.34	3.35	2.50	0.85
Concrete	9.57	7.71	7.33	5.47	1.86
Reinforced concrete	16.70	14.21	14.55	12.07	2.49

TABLE 3. Comparison of transmission and attenuation between L1 and L5/E5 frequencies

Building materials (excerpt)	Attenuation
Aluminium plate, thickness 1mm	> 50 dB
Steel grid, mesh 5 cm x 5 cm, 6 mm thick	7.5 dB
Steel grid, mesh 2.5 cm x 2.5 cm, 6 mm	21 dB
Chip board CE norm P3E1, 19 mm	0.9 dB
Tabletop, solid pine, thickness 35 mm	1.2 dB
Sheet glass, thickness 4 mm	0.3 dB
Window, heat protection glass, 1 m x 1m	17 dB
Aluminium jalousie, fins 25 mm, open	6 dB
Aluminium jalousie, fins 25 mm, closed	7 dB
Person in centre of measurement window	~ 6 dB

TABLE 4. Building materials and their attenuations at a frequency of 1500 MHz

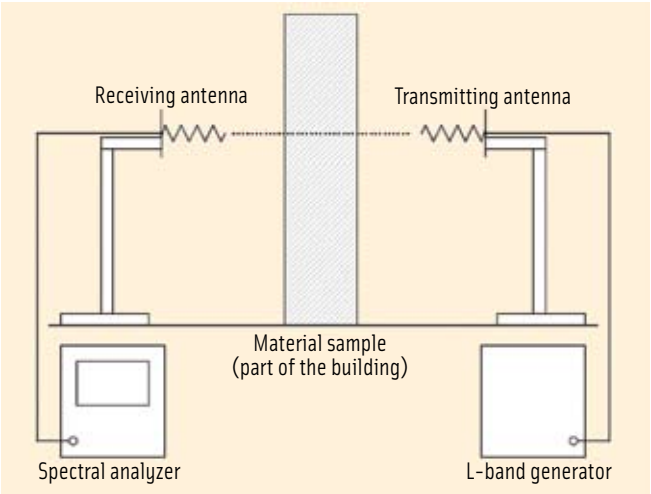

FIGURE 6 Measurement setup for the measurement of parts of the building

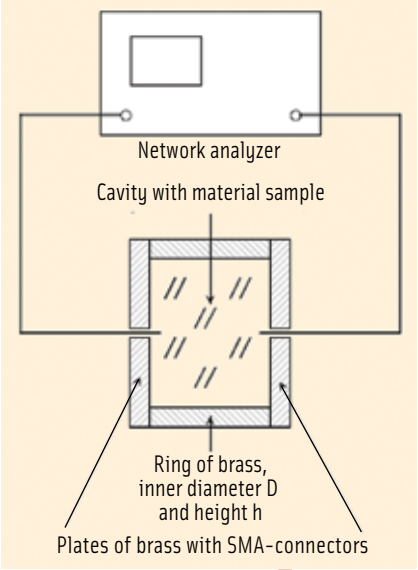

FIGURE 7 Measurement setup of resonator method

Part of Building	Attenuation
Brick wall with plaster on both sides, 24 cm	9 dB
Brick wall with plaster on both sides, 12 cm	5 dB
Sandstone brick, thickness 28 cm	4 dB
Massive concrete slab, 40 cm	14 dB
Massive concrete stair, 25 cm	15 dB
Slab, cavity block tiles and concrete, 23 cm	4 dB
Fire door, hardwood and glass 10 mm	4 dB
Special window, light + heat protection	27 dB

TABLE 5. Parts of buildings and their attenuations at the frequency 1757 MHz

Material	e′	e″
Iron Portland cement	7.6	1.1
Concrete (cement:sand 1:3)	3.36	0.12
Sand, waterless, dep. on compaction	2.34 – 2.54	0.008 – 0.01
Sand, 5% water, dep. on compaction	3.1 – 4.5	0.1 – 0.17
Plaster	3.4	0.057
Wood, spruce, humidity 8%	2.55	0.43
Wood, oak, humidity 9%	2.91	0.58
Mineral wool	1.03	0.003

TABLE 6. Measured materials and their permittivity values

For calibration of the measurement configuration, the signal levels at the three frequencies under investigation were measured with accurately adjusted antennas at distances ranging from six to eight meters. Then, we calculated the attenuation caused by each type of building material as being the differences between these reference levels and the levels measured when a piece of the material was located at the same distance within the signal path between the antennas. Results are shown in Table 5.

Case 3: Resonator Method

The third measurement configuration relied on a cylindrical resonator as the main equipment of interest (Figure 7). The theoretical fundamentals of this method were described in the publication by K. Kojucharow listed in the Additional Resources section at the end of this article. One main difference of the resonator method compared to the other two methods was that the permittivity components of raw materials were determined instead of the resulting attenuation.

This measurement approach exploited the resonator's implementation of a circular waveguide. Outputs included the resonant frequency f_r and the resonant wavelength λ_r of the relevant E-mode (here: E_{010}) and its quality factor Q_r. These two parameters served as input for the computation of the permittivity parameters ε' and ε''.

$$\varepsilon' = \left(\frac{c}{f_{r\,E_{010}} \cdot \lambda_{rE_{010}}} \right)^2 \qquad (19)$$

$$\varepsilon'' = \frac{\varepsilon'}{Q_{r\,E_{010}}} \qquad (20)$$

Some results from these measurements are presented in Table 6.

Conclusions

In the first of this three-part column, we presented a novel approach for a statistical channel model based on the well-known Saleh-Valenzuela model that has already been applied frequently in communications. Our approach was further enhanced by the fact that current elevation and azimuth of the satellite significantly affect the behaviour of the key parameters of the model that quantify the decay profiles.

Although the amount of data that we gathered was too sparse to be sure, it seems that the construction material of the building plays a minor role for the shape of the decay profiles. Of course, building materials affect the absolute power level of the signal to be received.

Thus, the second part of the column followed a more deterministic approach and started with an introduction on how the signal attenuation caused by a building can be computed on the basis of the dielectric properties of the materials with which it is constructed.

Simulations helped us understand what reinforced concrete really means to a GNSS signal. Furthermore, we introduced configurations of equipment and scenarios to measure relevant parameters of the building materials in order to fill the transmission model with practical input.

Having presented this synopsis on signal propagation through various

types of building materials, in the third and last part of the column we will turn to a future scenario: the propagation of an actual Galileo signal as it penetrates a building. In the next issue of *Inside GNSS,* we will present and discuss our analysis of experimental results performed by broadcasting the real modulated Galileo pilot signal on L1 and L5/E5 and measuring its reception inside a building.

Manufacturers

The RF network analyzer used in the free-field room tests was the E8361 made by **Agilent Technologies**, Santa Clara, California, USA. The spectrum analyzer used in the indoor test was an Agilent 8563EC. The portable spectrum analyzer used in the in-building tests was the FSH3 from **Rohde & Schwarz**, Munich, Germany. The L-band generator (based on the ADF4370-7 programmable integrated circuits made by **Analog Devices, Inc.**, Norwood, Massachusetts, USA) and the helical antennas were developed and designed by **KMDC – Kojucharow Microwave Development and Consulting,** Dresden, Germany.

Additional Resources

Kojucharow, K., *Determination of Complex Dielectric Constant Using Cylindrical Resonator Method*. Design Note Nr. 2, KMDC Dresden, 2007

Authors

"Working Papers" explore the technical and scientific themes that underpin GNSS programs and applications. This regular column is coordinated by **PROF. DR.-ING. GÜNTER HEIN.** Prof. Hein is a member of the European Commission's Galileo Signal Task Force and organizer of the annual Munich Satellite Navigation Summit. He has been a full professor and director of the Institute of Geodesy and Navigation at the University of the Federal Armed Forces Munich (University FAF Munich) since 1983. In 2002, he received the United States Institute of Navigation Johannes Kepler Award for sustained and significant contributions to the development of satellite navigation. Hein received his Dipl.-Ing and Dr.-Ing. degrees in geodesy from the University of Darmstadt, Germany. Contact Prof. Hein at <Guenter.Hein@unibw-muenchen.de>.

Andreas Teuber is research associate at the Institute of Geodesy and Navigation at the University FAF Munich. He received his diploma in geomatics engineering from the University of Hannover, Germany. Currently, his main subjects of interest are indoor positioning in general and applying WLAN technology for positioning purposes in particular.

Anne Wolf received her M.S. degree in electrical engineering from the Dresden University of Technology, Germany. Now, she is with the Communications Laboratory in the Department of Electrical Engineering and Information Technology at the Dresden University of Technology and is working towards her Ph.D. degree. Her research interests are focused on channel coding, digital signal processing, and information theory in wireless communication.

Hans-Jörg Thierfelder received the Dr.-Ing. and Dr.-Ing. habil. degrees in information technology from Dresden University of Technology. In 1970 he joined Communications Laboratory of Dresden University of Technology where he worked as a research assistant. Now he is working as lecturer and research associate. His research interests include digital signal processing, wireless communication, and network theory. IG